Department of Medicine Publications   Medicine Department

8-1-2008

Geometry of the carotid bifurcation predicts its exposure to disturbed flow

Sang Wook Lee
University of Toronto

Luca Antiga
Istituto di Ricerche Farmacologiche Mario Negri

J. David Spence
Robarts Research Institute

David A. Steinman
University of Toronto

Geometry of the Carotid Bifurcation Predicts Its Exposure to Disturbed Flow

Sang-Wook Lee, PhD; Luca Antiga, PhD; J. David Spence, MD; David A. Steinman, PhD

Background and Purpose—That certain vessels might be at so-called geometric risk of atherosclerosis rests on assumptions of wide interindividual variations in disturbed flow and of a direct relationship between disturbed flow and lumen geometry. In testing these often-implicit assumptions, the present study aimed to determine whether investigations of local risk factors in atherosclerosis can indeed rely on surrogate geometric markers of disturbed flow.

Methods—Computational fluid dynamics simulations were performed on carotid bifurcation geometries derived from MRI of 25 young adults. Disturbed flow was quantified as the surface area exposed to low and oscillatory shear beyond objectively-defined thresholds. Interindividual variations in disturbed flow were contextualized with respect to effects of uncertainties in imaging and geometric reconstruction. Relationships between disturbed flow and various geometric factors were tested via multiple regression.

Results—Relatively wide variations in disturbed flow were observed among the 50 vessels. Multiple regression revealed a significant ($P < 0.002$) relationship between disturbed flow and both proximal area ratio ($\beta \approx 0.5$) and bifurcation tortuosity ($\beta \approx -0.4$), but not bifurcation angle, planarity, or distal area ratio. These findings were shown to be insensitive to assumptions about the flow conditions and to the choice of disturbed flow indicator and threshold.

Conclusions—Certain geometric features of the young adult carotid bifurcation are robust surrogate markers of its exposure to disturbed flow. It may therefore be reasonable to consider large-scale retrospective or prospective imaging studies of local risk factors for atherosclerosis without the need for time-consuming and expensive flow imaging or CFD studies. (***Stroke***. 2008;39:2341-2347.)

That atherosclerotic plaques are focal, tending to occur near arterial bifurcations and bends, has led to the widely accepted idea that hemodynamic forces (particularly wall shear stresses) play an important role in the development and progression of atherosclerosis.[1] Because these forces are determined primarily by lumen geometry, it has been suggested that certain individuals might be at increased risk of developing atherosclerosis by virtue of their particular arterial geometry.[2]

These local risk hypotheses are predicated on the assumption of wide interindividual variations in exposure to "disturbed" blood flow, something yet to be tested rigorously. (The imprecise nature of the term "disturbed" has been discussed by Himburg and Friedman[3]; for the remainder of this article the quotation marks are implied.) Instead, Schulz and Rothwell demonstrated wide variations in the relative dimensions of carotid bifurcation of older adults with <30% stenosis[4]; however, our group subsequently found significantly narrower variations in the geometries of ostensibly healthy young adults.[5]

The geometric risk hypothesis also hinges on the assumption of a direct relationship between exposure to disturbed flow and purported geometric risk factors. This too has not been tested directly. Rather, it has been intuited from parametric studies of often-idealized vascular models for which geometric factors have been varied independently.[6–8] The power of such relationships, if indeed they exist, remains unclear, which may explain the lack of consensus regarding the role of geometric factors in the development of atherosclerosis.

The objective of this study was therefore to test these often-implicit assumptions in a statistically meaningful manner. In so doing, we aimed to determine whether investigations of local risk factors can indeed rely on the use of surrogate geometric markers of disturbed flow.

Subjects and Methods

The "subjects" of this study were 50 carotid bifurcation lumen geometries digitally reconstructed from black blood MRI of 25 ostensibly healthy volunteers (24±4 years; range, 19 to 38 years; 14:11 M:F), whose carotid bifurcation geometries were presumably
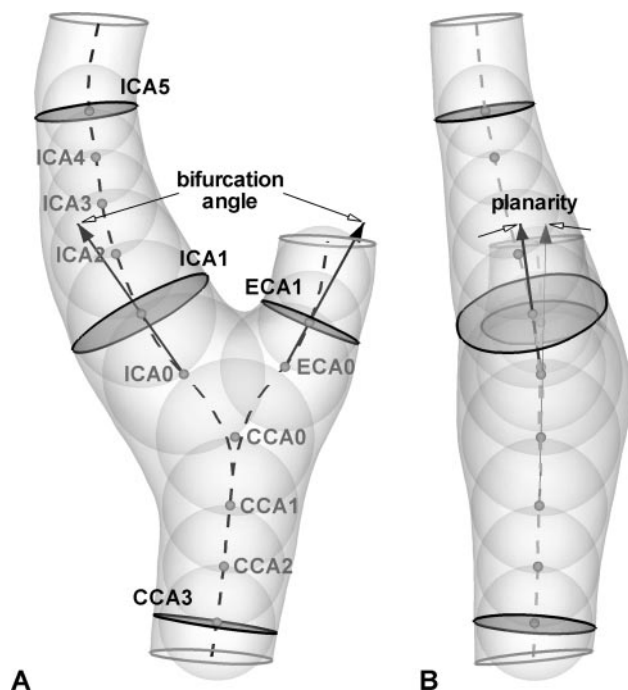
Figure 1. Representative normal carotid bifurcation, showing vessel centerlines (dashed) and the maximally-inscribed spheres used to define distances along the vessel branches, from which various geometric factors are derived. For example, ICA5 refers to a point exactly 5 sphere radii along the ICA centerline starting from the ICA origin (ie, ICA0). Transverse sections through CCA3, ICA1, ICA5, and ECA1 were those used to compute the area ratios. It is worth noting that the various entities depicted (and hence the derived geometric factors) are all generated from the lumen surface automatically, according to operator-independent criteria.
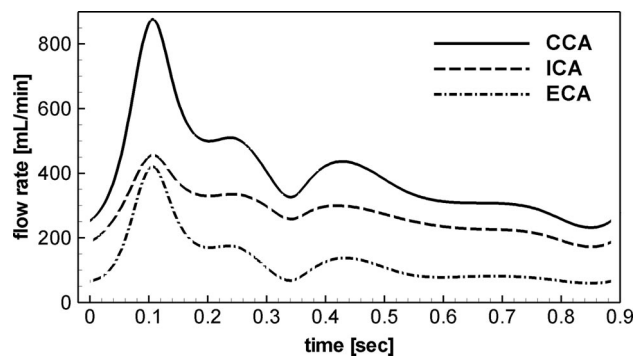

Figure 2. Flow rate waveforms corresponding to average CCA and ICA dimensions. Heart rate is 68 bpm and mean flow rates are 407 mL/min (CCA), 277 mL/min (ICA), and 130 mL/min (ECA). As detailed in the Methods, these mean flow rates were adapted to the CCA3 and ICA5 dimensions for each case.

free of secondary effects of atherosclerosis. A representative geometry is presented in Figure 1, which also shows transverse sections through the common (CCA), internal (ICA), and external (ECA) carotid arteries used for later quantitative analysis. Details of the imaging and lumen reconstruction, as well as the definition and extraction of these sections, are provided elsewhere.[5] The present study was approved by an institutional review committee, and all subjects gave informed consent.

Computational Fluid Dynamics

Pulsatile blood flow dynamics were simulated for each of the 50 carotid bifurcation geometries using a well-validated finite-element-based computational fluid dynamics (CFD) solver.[9–11] Quadratic tetrahedral-element meshes were generated by a commercial mesh generator (ICEM-CFD; ANSYS) using a uniform node spacing of 0.2 mm, previously shown to be sufficient for resolving wall shear stresses.[12] Fully-developed (Womersley) velocity boundary conditions were imposed at the CCA inlet and ECA outlet; traction-free boundary conditions were imposed at the ICA outlet. Rigid walls and a constant blood viscosity of 3.5 mm²/s were assumed. Further details of the meshing and specification of boundary conditions are provided elsewhere.[12]

Flow rates were not available for these subjects, so inlet/outlet pulsatile flow rates were defined for each case based on the following observations: flow waveform *shape* is relatively consistent across normal subjects[13]; and mean flow rate scales approximately with lumen cross-sectional area.[14] Inlet/outlet flow rate waveforms were first defined for an *average* case by combining the normal ICA flow waveform of Ford et al[13] with the time-varying ICA:CCA flow division data of Marshall et al[15] (Figure 2). Then, for each *individual* case, these average CCA and ICA waveforms were scaled by,

respectively, the ratios of the CCA3 and ICA5 cross-sectional areas (see Figure 1) to their respective averages over the 50 cases. The individual ECA waveform was then calculated as the difference between the individual CCA and ICA waveforms. The present study focused on simulations carried out using these scaled flow rates; however, simulations were also carried out using the same average flow waveforms (ie, those in Figure 2) across *all* 50 cases, as a way of testing the sensitivity of the findings to the assumed flow conditions.

CFD simulations were carried out using up to 4800 timesteps per cardiac cycle, and 3 cycles were required to damp initial transients. For each CFD model we then computed the surface distributions of the following hemodynamic parameters: time-averaged wall shear stress magnitude (WSS) and oscillatory shear index (OSI). OSI, a measure of directional changes in wall shear stress over the cardiac cycle, is a dimensionless quantity. WSS, on the other hand, is a dimensional quantity, and its baseline value depends on an individual's vessel size and flow rate. For this reason, and consistent with the notion of disturbed flow as "flow that differs from the 'undisturbed' pulsatile flow that is seen in relatively straight vessel segments,"[3] for each case WSS was normalized by its nominal value at the respective CCA3 section. To ensure a consistent axial extent for all cases—the length of each model depended on the number of MRI slices acquired for each subject—each CFD model was clipped at its respective CCA3 and ICA5 sections before further quantitative analysis.

Quantification of Disturbed Flow

While it is widely accepted that low and oscillatory shear promotes an atherogenic endothelial cell phenotype,[1] there remains no definitive quantitative relationship between disturbed flow and risk of atherosclerosis. Following the approach of Stone et al,[16] we pooled together the surfaces of all 50 models, and identified threshold values of OSI and normalized WSS to which up to 80% or 90% of this cumulative surface was exposed. (Two different percentiles were chosen to test the sensitivity of the findings to choice of threshold.) Then, for a given model, disturbed flow was quantified as its surface area (SA) exposed to normalized WSS below (or OSI above) the respective threshold values. Finally, to factor out the influence of vessel size—for the same geometry, a larger vessel will experience more disturbed flow—a *relative* exposure (SA_{rel}) was defined as this absolute exposure (SA_{abs}) divided by the total surface area of the respective model.

Quantification of Geometry

A variety of geometric factors defining each bifurcation was extracted automatically, as described previously.[5] Here we focused on those factors characterizing the bifurcation as a whole (Figure 1): angle, planarity, tortuosity, and area ratio. Tortuosity was defined as L/D-1, where L is the length of the centerline from CCA3 to ICA5,

and D is the straight-line distance between these 2 points. (Tortuosity may thus be thought of as the fractional extra distance blood must travel in the real vessel versus a theoretical, straight-line path.) Previously, area ratio was defined as the sum of the ECA1 and distal ICA5 section areas, divided by the CCA3 section area, these locations chosen to be consistent with Schulz and Rothwell.[4] Noting that disturbed flow typically occurs near the level of the flow divider, the present study also defined an area ratio using the more proximal ICA1 section instead. Hereafter these distal and proximal area ratios are referred to as AR5 and AR1, reflecting the ICA section used in their respective definitions. Descriptive statistics for tortuosity and AR1 were 0.025 ± 0.018 (range 0.009 to 0.058) and 1.82 ± 0.28 (range 1.17 to 2.42), respectively (see Thomas et al[5] for angle, planarity, and AR5).

Statistical Analysis

Interindividual variations were quantified as the standard deviations of both SA_{abs} and SA_{rel} across the 50 cases. The magnitude of these variations was contextualized by similarly calculating these quantities for 3 separate cases for which reproducibility of the entire image-based CFD process was previously assessed via 3 repeated acquisitions.[17] Specifically, *intraindividual* variations were quantified as the square root of the within-subject variances in SA_{abs} and SA_{rel} averaged across those 3 subjects.

Multiple linear regression was used to quantify the relationship between exposure to disturbed flow (SA_{rel}) and angle, planarity, tortuosity, and either of AR5 or AR1 as independent predictors. The overall quality of the regression was assessed using Pearson's correlation coefficient, adjusted by the number of independent predictors (R^2_{adj}). The relative contributions of the geometric predictors was determined from the standardized (β) regression coefficients.

These analyses were performed separately for the 4 permutations of hemodynamic parameter and threshold criterion (hereafter identified as WSS80, WSS90, OSI80, and OSI90) to test the sensitivity of findings to the choice of disturbed flow indicator. Statistical analyses were carried out using Microsoft Excel 2003 with StatistiXL v1.7 add-on.

Results

Interindividual Variations in Disturbed Flow

Figure 3 confirms, qualitatively at least, the wide interindividual variations in low and oscillating shear among the 50 normal carotid bifurcations studied. Models for some cases (eg, 2L and 24R) showed almost no disturbed flow, whereas for others (eg, 11L and 23L) much of the bifurcation region was exposed to disturbed flow. Still, in most cases, disturbed flow was concentrated around the outer walls of the ICA and ECA as expected.[18,19] Moreover, on a case-by-case basis, the extent and distribution of low normalized WSS appeared to largely mirror that of high OSI, which was confirmed by correlation analysis: Pearson R^2 values were 0.642 (WSS80 versus OSI80) and 0.526 (WSS90 versus OSI90), both highly significant ($P < 0.0001$).

As enumerated in Table 1, interindividual variations in disturbed flow were uniformly above the level of intraindividual variations attributable to uncertainty in the CFD model geometries, irrespective of the threshold or hemodynamic parameter. As quantified by SA_{abs}, these interindividual variations were typically 2 to 3 times greater than the intraindividual variations. Even after adjusting for individual vessel size, interindividual variations in SA_{rel} were still 1.5 to 2 times greater.

Relationship Between Geometry and Disturbed Flow

As summarized in Table 2, multiple regressions revealed a significant inverse relationship between exposure to disturbed flow and vessel tortuosity, but not angle, planarity or *distal* area ratio (AR5), irrespective of the hemodynamic parameter or threshold criterion. Multiple regressions using AR1 instead of AR5 (Table 3) revealed that the combination of tortuosity and proximal area ratio was a far stronger predictor of exposure to disturbed flow.

Discussion

The present study has demonstrated wide interindividual variations in the exposure of the young adult carotid bifurcation to disturbed flow—at least wide with respect to variations that could be attributed to uncertainty in imaging and reconstruction processes. This is significant, because our previous work had suggested the difficulty of reconciling narrow variations in young adult carotid bifurcation geometry with the concept of local risk for atherosclerosis.[5] Nevertheless, although our findings are consistent with this idea, in no way do they prove it.

Of course, the presence of wide variations in normal carotid bifurcation hemodynamics is widely appreciated, especially by sonographers and radiologists, as demonstrated by Steinke and colleagues.[19] In that study, disturbed flow was assessed semiquantitatively from the durations and extents of retrograde flow observed in 2-dimensional longitudinal and cross-sectional color Doppler ultrasound images. In the present study, a combination of MRI and CFD was used to determine the 3-dimensional distributions and relative intensities of the disturbed wall shear stresses themselves.

More importantly, our study has shown that the exposure of an individual carotid bifurcation to disturbed flow can be predicted by a relatively simple relationship:

$$SA_{rel} \propto AR1 - C \times \text{Tortuosity}$$

where C is a positive constant falling between 19 and 27, depending on the choice of disturbed flow indicator. In other words, bifurcations with larger proximal area ratios are more susceptible to disturbed flow, but this can be ameliorated by the presence of a curved or tortuous path along the CCA and ICA. Proximal area ratio (AR1) may itself be viewed as a measure of bifurcation flare, which is well known to promote flow separation,[20] the consequence of which is low and oscillating shear. Similarly, tortuosity may be seen as an indirect marker of swirling flow, which can be instrumental in suppressing flow disturbances[21] (and perhaps their consequences[22]).

The finding of a significant relationship between area ratio and exposure to disturbed flow echoes conclusions drawn from idealized model studies.[6,23] On the other hand, previous model studies had also suggested an important role for branch angle,[8] which is contrary to our finding here. This may be attributed to the fact that only angle was varied in that study, whereas, strictly speaking, one would have to probe an N-dimensional space of *possible* geometries to investigate the *relative* importance of N parameters. For example, Karino and Goldsmith demonstrated the relative importance of di-
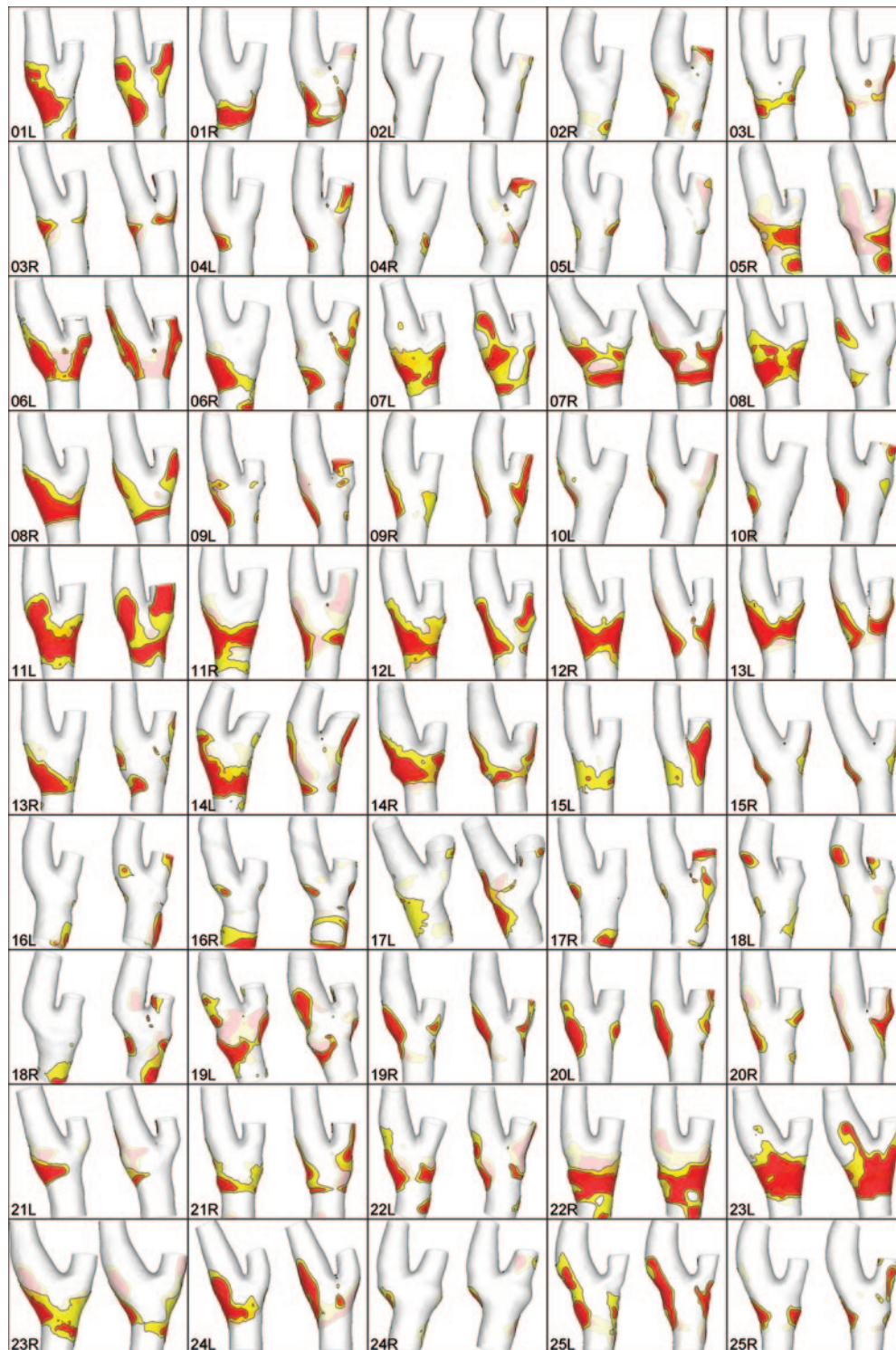
Figure 3. Wide interindividual variations in exposure to low and oscillating shear for the 50 cases, identified at the bottom left of each panel. Dark (red) highlights those areas exposed to low normalized WSS (left of each panel) and high OSI (right of each panel) outside the 90th percentile. The lighter (yellow) penumbra incorporates areas exposed outside the 80th percentile. Translucent rendering highlights disturbed flow on the back walls of the models. CFD models are shown clipped at the CCA3 and ICA5 sections and not necessarily to the same physical scale. The full CFD domains are shown to scale in Thomas et al.[5]

ameter ratio versus angle on vortex formation using an idealized bifurcation geometry for which those two geometric parameters were each varied over a wide range.[23] Here we were able to efficiently sample a potentially huge

4-dimensional parameter space by using a representative set of *actual* carotid bifurcation geometries.

Our results are also consistent with the geometric risk study of Fisher and Fieman,[24] which found that intraindi-

Table 1. Descriptive Statistics (mean±SD) for Exposure to Disturbed Flow

	Interindividual (n=50)			Intraindividual (n=3×3)		
	Threshold Value	SA_abs (mm²)	SA_rel (%)	Threshold Value	SA_abs (mm²)	SA_rel (%)
WSS80	0.481	134±79	19.4±10.3	0.930	124±27	19.9±4.6
WSS90	0.334	66±51	9.5±7.1	0.648	65±21	10.2±3.7
OSI80	0.145	138±67	19.6±7.8	0.057	120±24	19.4±3.9
OSI90	0.238	69±42	9.8±5.2	0.116	62±19	10.0±3.4

vidual asymmetry in stenosis severity was associated with area ratio asymmetry, but not branch angle asymmetry. In an earlier study,[25] Harrison and Marshall found no significant difference between the bifurcation angles of normal patients versus those with (angiographic) plaque, but noted "the line of the common carotid and internal carotid artery was straighter in those with atheroma," consistent with our finding of a significant inverse relationship between ICA-CCA tortuosity and disturbed flow. On the other hand Smedby and Bergstrand demonstrated the influence of tortuosity on the development of atherosclerosis[26]; however, that study was confined to nonbranching femoral arteries.

As might be anticipated from its definition, we noted a correlation between tortuosity and ICA-CCA angle (Pearson R^2=0.392; P<0.0001), which itself was weakly correlated with bifurcation angle (Pearson R^2=0.145; P=0.0064). Repeating the multiple regressions with ICA-CCA angle and AR1 as independent predictors maintained the strong relationship between SA_rel and AR1; however, β for the ICA-CCA angle was around −0.25 and not significant (c.f., $\beta_{Tortuosity}$≈−0.4 and highly significant per Table 3). This reinforces the idea—and our finding—that branch angles are not particularly strong predictors of disturbed flow. Similarly, the lack of an association between disturbed flow and planarity is consistent with previous work showing that "bending" individual carotid bifurcations onto their respective bifurcation planes had no consistent effect on the distributions of low and oscillating shear.[27]

Modeling Assumptions and Potential Shortcomings

As noted in the Methods, a number of modeling assumptions (rigid walls, Newtonian rheology, fully-developed entry flow) were made to render the analysis tractable. These were considered reasonable, in the sense that they have been shown to have only a minor effect on the resulting carotid bifurcation flow dynamics.[12,28–30] On the other hand, although it is widely accepted that flow rate has a similarly minor influ-

ence,[31] we considered the possibility that our findings were biased by our assumed flow conditions.

Use of fixed flow waveform shapes was justified by the observation that interindividual variations in carotid flow rate dynamics can be attributed mainly to variations in mean flow; variations in waveform *shape* are close to the level of measurement uncertainty or normal physiological fluctuations.[13,32] Implicit in the use of fixed waveform shapes is a fixed heart rate, here set to 68 bpm. Younis et al[33] reported "minimal" changes in OSI for a carotid bifurcation model exposed to resting (72 bpm) versus exercise (104 bpm) conditions, suggesting that the effect of more modest normal variations in heart rate can be considered negligible.

What remains then is the reliance on a scaling law to estimate the mean flow rates for each subject. Regarding the choice of scaling law (ie, flow rate scales with cross-sectional area[14]), we note that interindividual variations among the n=50 anatomically-scaled ICA flow rates (σ=54 mL/min, range 181 to 416) were remarkably consistent with interindividual variations in flow rates measured by phase contrast MRI (PC-MRI) in a separate group of n=17 young adults (σ=56 mL/min, range 167 to 445).[13] Similarly, variations in the scaled ICA:CCA flow ratios (σ=0.10, range 0.49 to 0.91) compared favorably with those derived from independent PC-MRI measurements (σ=0.098, range 0.58 to 0.89; Dr Ian Marshall, unpublished data, 2007).

Although this circumstantial evidence supports our choice of scaling law, it ultimately says little about the sensitivity of our findings to the assumed flow rates and flow divisions. As noted in the Methods, to test this more directly we applied the same flow conditions across *all* 50 cases. As presented in the supplemental data (supplemental Figure I and supplemental Table I, available online at http://stroke.ahajournals.org), the qualitative and quantitative findings based on the assumption of uniform flow were virtually identical to those based on the assumption of anatomically-scaled flow (Figure 3 and Table 3, respectively). This confirms the robustness of our findings

Table 2. Multiple Regressions of Exposure to Disturbed Flow (SA_rel), With Angle, Planarity, Tortuosity, and Distal Area Ratio (AR5) as Independent Predictors

	Model Quality		Standardized Coefficients							
	R^2_{adj}	P Value	β_{Angle}	P Value	$\beta_{Planarity}$	P Value	$\beta_{Tortuosity}$	P Value	β_{AR5}	P Value
WSS80	0.115	0.049	0.123	NS (0.38)	0.032	NS (0.82)	−0.444	0.0028	0.062	NS (0.66)
WSS90	0.127	0.038	0.074	NS (0.59)	−0.047	NS (0.74)	−0.442	0.0028	0.114	NS (0.42)
OSI80	0.122	0.042	0.139	NS (0.90)	0.178	NS (0.32)	−0.412	0.0051	0.207	NS (0.14)
OSI90	0.174	0.013	0.228	NS (0.10)	0.105	NS (0.44)	−0.472	0.0011	0.146	NS (0.29)

Table 3. Multiple Regressions of Exposure to Disturbed Flow After Replacing Distal Area Ratio (AR5) With Proximal Area Ratio (AR1)

	Model Quality		Standardized Coefficients							
	R^2_{adj}	P Value	β_{Angle}	P Value	$\beta_{Planarity}$	P Value	$\beta_{Tortuosity}$	P Value	β_{AR1}	P Value
WSS80	0.291	0.0006	−0.042	NS (0.76)	0.064	NS (0.61)	−0.456	0.0006	0.443	0.0015
WSS90	0.362	<0.0001	−0.113	NS (0.38)	−0.018	NS (0.88)	−0.449	0.0004	0.518	0.0001
OSI80	0.319	0.0002	−0.033	NS (0.80)	0.188	NS (0.13)	−0.401	0.0019	0.512	0.0003
OSI90	0.315	0.0003	0.082	NS (0.53)	0.118	NS (0.34)	−0.468	0.0004	0.422	0.0021

to the assumed flow conditions and further reinforces the primacy of geometry in determining exposure of a vessel to disturbed flow.

Aside from the modeling assumptions, a potential shortcoming was that *intraindividual* variations used to contextualize our findings were based on data from a separate reproducibility study of three ostensibly normal, but elderly (74 to 77 years), subjects.[17] Those subjects tended to have less disturbed flow, as evidenced by the higher normalized WSS and lower OSI threshold values enumerated in Table 1. Nevertheless, these data likely provide a conservative estimate of intraindividual variability for young adults since, in our experience anyway, image quality (and hence reconstruction variability) tends to be poorer for older subjects.

By design, our study also did not consider the spatial distribution of disturbed flow. For example, as demonstrated by Steinke and colleagues,[19] and consistent with Figure 3, disturbed flow tends to be ICA-dominant, although often it is distributed circumferentially around the bifurcation. (Interestingly, those authors also noted an association between flow separation and carotid bulb size, but not bifurcation angle, which parallels our finding of a relationship between SA_{rel} and AR1, but not bifurcation angle.) In fact, repeating the multiple regressions using the ICA1:CCA3 area ratio (namely, the relative bulb size) instead of the (ICA1+ECA1):CCA3 area ratio (ie, AR1), we found comparable relationships to SA_{rel}, albeit marginally weaker (eg, for WSS90, R^2_{adj}=0.329 versus 0.361). Further investigations may therefore reveal geometric factors that give rise to differential spatial distributions of disturbed flow, which might be particularly useful for studies in which the distribution of early wall thickening shows comparable spatial variations.

Finally, absent a definitive quantitative relationship between disturbed flow and atherosclerosis risk, our study was forced to rely on a simple, threshold-based criterion to discriminate disturbed flow, albeit one informed by broadly-accepted qualitative criteria,[3] and consistent with previous work.[16] Nevertheless, our findings were robust to reasonable choices for the percentile-based thresholds. Our findings were also robust to the choice of hemodynamic parameter, although this was almost certainly a reflection of a strong correlation between normalized WSS and OSI. Although low and oscillatory shear is widely thought to promote endothelial dysfunction,[1] there are other disturbed flow indicators (eg, based on WSS gradients,[34] residence times,[35] or WSS harmonic content[3,36]) that may ultimately be more closely linked to the underlying mechanisms. However, these too may also

be strongly inter-related,[37] something we are presently investigating with our models.

Implications for Geometric/Hemodynamic Risk of Atherosclerosis

As noted above, the present study neither proves nor disproves the notion that individuals may be exposed to differential risk of atherosclerosis by virtue of their local arterial geometry or hemodynamics. Rather, like Schulz and Rothwell,[4] we have confirmed a necessary, but not sufficient, condition for this local risk hypothesis, in this case that there do exist wide interindividual variations in exposure to disturbed flow. Moreover, this was demonstrated in a group for which secondary effects of atherosclerosis on geometry were presumably negligible.

A less abstract and more immediate implication of our findings is that, for studies aimed at elucidating the role of local risk factors in atherosclerosis, it may be unnecessary to acquire local hemodynamic data. This is important, as direct imaging of carotid bifurcation wall shear stresses remains a significant challenge.[38] Similarly, although great advances have been made in the area of image-based CFD,[39] such models usually require additional imaging data and remain cumbersome to construct and use. Historically, these constraints have made it difficult to carry out studies of sufficient size to control for other systemic risk factors. On the other hand, noninvasive, 3-dimensional imaging of the carotid bifurcation is becoming increasingly available and practical.[40] This opens up the possibility of retrospective studies of local risk factors in atherosclerosis using routinely-acquired clinical images, or prospective studies where it might not be easy or cost-effective to acquire the data necessary for quantifying disturbed flow.

Lastly, it must be stressed that our findings in no way imply that the complexities of carotid bifurcation blood flow dynamics can be encoded into simple geometric factors such as area ratio or tortuosity. Rather, much like stenosis severity and aneurysm size are useful surrogate geometric markers of plaque and aneurysm rupture risk despite only crudely approximating the biophysical factors that ultimately lead to rupture, the use of area ratio and tortuosity is being proposed here as a pragmatic solution to the problem of quantifying disturbed flow for future, evidence-based studies of local risk factors for atherosclerosis.

Disclosures

None.

References

1. Malek AM, Alper SL, Izumo S. Hemodynamic shear stress and its role in atherosclerosis. *JAMA*. 1999;282:2035–2042.
2. Friedman MH, Deters OJ, Mark FF, Bargeron CB, Hutchins GM. Arterial geometry affects hemodynamics. A potential risk factor for atherosclerosis. *Atherosclerosis*. 1983;46:225–231.
3. Himburg HA, Friedman MH. Correspondence of low mean shear and high harmonic content in the porcine iliac arteries. *J Biomech Eng*. 2006;128:852–856.
4. Schulz UG, Rothwell PM. Major variation in carotid bifurcation anatomy: a possible risk factor for plaque development? *Stroke*. 2001;32:2522–2529.
5. Thomas JB, Antiga L, Che SL, Milner JS, Hangan-Steinman DA, Spence JD, Rutt BK, Steinman DA. Variation in the carotid bifurcation geometry of young versus older adults: implications for geometric risk of atherosclerosis. *Stroke*. 2005;36:2450–2456.
6. Friedman MH, O'Brien V, Ehrlich LW. Calculations of pulsatile flow through a branch: implications for the hemodynamics of atherogenesis. *Circ Res*. 1975;36:277–285.
7. Motomiya M, Karino T. Flow patterns in the human carotid artery bifurcation. *Stroke*. 1984;15:50–56.
8. Perktold K, Peter RO, Resch M, Langs G. Pulsatile non-Newtonian blood flow in three-dimensional carotid bifurcation models: a numerical study of flow phenomena under different bifurcation angles. *J Biomed Eng*. 1991;13:507–515.
9. Ethier CR, Steinman DA, Ojha M. Comparisons between computational hemodynamics, photochromic dye flow visualization and magnetic resonance velocimetry. In: Xu XY, Collins MW, eds. *The Haemodynamics of Arterial Organs–Comparison of Computational Predictions with In Vivo and In Vitro Data*. Southampton: WIT Press; 1999.
10. Minev PD, Ethier CR. A characteristic/finite element algorithm for the 3-D Navier-Stokes equations using unstructured grids. *Comput Meth Appl Mech Eng*. 1999;178:39–50.
11. Ethier CR, Prakash S, Steinman DA, Leask RL, Couch GG, Ojha M. Steady flow separation patterns in a 45 degree junction. *J Fluid Mech*. 2000;411:1–38.
12. Moyle KR, Antiga L, Steinman DA. Inlet conditions for image-based CFD models of the carotid bifurcation: is it reasonable to assume fully developed flow? *J Biomech Eng*. 2006;128:371–379.
13. Ford MD, Alperin N, Lee SH, Holdsworth DW, Steinman DA. Characterization of volumetric flow rate waveforms in the normal internal carotid and vertebral arteries. *Physiol Meas*. 2005;26:477–488.
14. Weinberg PD, Ethier CR. Twenty-fold difference in hemodynamic wall shear stress between murine and human aortas. *J Biomech*. 2007;40:1594–1598.
15. Marshall I, Papathanasopoulou P, Wartolowska K. Carotid flow rates and flow division at the bifurcation in healthy volunteers. *Physiol Meas*. 2004;25:691–697.
16. Stone PH, Coskun AU, Kinlay S, Clark ME, Sonka M, Wahle A, Ilegbusi OJ, Yeghiazarians Y, Popma JJ, Orav J, Kuntz RE, Feldman CL. Effect of endothelial shear stress on the progression of coronary artery disease, vascular remodeling, and in-stent restenosis in humans: in vivo 6-month follow-up study. *Circulation*. 2003;108:438–444.
17. Thomas JB, Milner JS, Rutt BK, Steinman DA. Reproducibility of image-based computational fluid dynamics models of the human carotid bifurcation. *Ann Biomed Eng*. 2003;31:132–141.
18. Zarins CK, Giddens DP, Bharadvaj BK, Sottiurai VS, Mabon RF, Glagov S. Carotid bifurcation atherosclerosis. Quantitative correlation of plaque localization with flow velocity profiles and wall shear stress. *Circ Res*. 1983;53:502–514.
19. Steinke W, Kloetzsch C, Hennerici M. Variability of flow patterns in the normal carotid bifurcation. *Atherosclerosis*. 1990;84:121–127.
20. MacLean NF, Roach MR. Thickness, taper, and ellipticity in the aortoiliac bifurcation of patients aged 1 day to 76 years. *Heart Vessels*. 1998;13:95–101.
21. Caro CG, Doorly DJ, Tarnawski M, Scott KT, Long Q, Dumoulin CL. Non-planar curvature and branching of arteries and non-planar-type flow. *Proc R Soc Lond A*. 1996;452:185–197.
22. Huijbregts HJ, Blankestijn PJ, Caro CG, Cheshire NJ, Hoedt MT, Tutein Nolthenius RP, Moll FL. A helical PTFE arteriovenous access graft to swirl flow across the distal anastomosis: results of a preliminary clinical study. *Eur J Vasc Endovasc Surg*. 2007;33:472–475.
23. Karino T, Goldsmith HL. Particle flow behavior in models of branching vessels. II. Effects of branching angle and diameter ratio on flow patterns. *Biorheology*. 1985;22:87–104.
24. Fisher M, Fieman S. Geometric factors of the bifurcation in carotid atherogenesis. *Stroke*. 1990;21:267–271.
25. Harrison MJG, Marshall J. Does the geometry of the carotid bifurcation affect its predisposition to atheroma? *Stroke*. 1983;14:117–118.
26. Smedby O, Bergstrand L. Tortuosity and atherosclerosis in the femoral artery: what is cause and what is effect? *Ann Biomed Eng*. 1996;24:474–480.
27. Thomas JB, Milner JS, Steinman DA. On the influence of vessel planarity on local hemodynamics at the human carotid bifurcation. *Biorheology*. 2002;39:443–448.
28. Zhao SZ, Xu XY, Collins MW, Stanton AV, Hughes AD, Thom SA. Flow in carotid bifurcations: effect of the superior thyroid artery. *Med Eng Phys*. 1999;21:207–214.
29. Younis HF, Kaazempur-Mofrad MR, Chan RC, Isasi AG, Hinton DP, Chau AH, Kim LA, Kamm RD. Hemodynamics and wall mechanics in human carotid bifurcation and its consequences for atherogenesis: investigation of inter-individual variation. *Biomech Model Mechanobiol*. 2004;3:17–32.
30. Lee SW, Steinman DA. On the relative importance of rheology for image-based CFD models of the carotid bifurcation. *J Biomech Eng*. 2007;129:273–278.
31. Friedman MH, Giddens DP. Blood flow in major blood vessels-modeling and experiments. *Ann Biomed Eng*. 2005;33:1710–1713.
32. Holdsworth DW, Norley CJ, Frayne R, Steinman DA, Rutt BK. Characterization of common carotid artery blood-flow waveforms in normal human subjects. *Physiol Meas*. 1999;20:219–240.
33. Younis HF, Kaazempur-Mofrad MR, Chung C, Chan RC, Kamm RD. Computational analysis of the effects of exercise on hemodynamics in the carotid bifurcation. *Ann Biomed Eng*. 2003;31:995–1006.
34. Kleinstreuer C, Hyun S, Buchanan JR Jr, Longest PW, Archie JP Jr, Truskey GA. Hemodynamic parameters and early intimal thickening in branching blood vessels. *Crit Rev Biomed Eng*. 2001;29:1–64.
35. Himburg HA, Grzybowski DM, Hazel AL, LaMack JA, Li XM, Friedman MH. Spatial comparison between wall shear stress measures and porcine arterial endothelial permeability. *Am J Physiol Heart Circ Physiol*. 2004;286:H1916–H1922.
36. Gelfand BD, Epstein FH, Blackman BR. Spatial and spectral heterogeneity of time-varying shear stress profiles in the carotid bifurcation by phase-contrast MRI. *J Magn Reson Imaging*. 2006;24:1386–1392.
37. Friedman MH, Deters OJ. Correlation among shear rate measures in vascular flows. *J Biomech Eng*. 1987;109:25–26.
38. Papathanasopoulou P, Zhao S, Kohler U, Robertson MB, Long Q, Hoskins P, Xu XY, Marshall I. MRI measurement of time-resolved wall shear stress vectors in a carotid bifurcation model, and comparison with CFD predictions. *J Magn Reson Imaging*. 2003;17:153–162.
39. Steinman DA. Image-based computational fluid dynamics: A new paradigm for monitoring hemodynamics and atherosclerosis. *Curr Drug Targets Cardiovasc Hematol Disord*. 2004;4:183–197.
40. Wardlaw JM, Chappell FM, Stevenson M, De Nigris E, Thomas S, Gillard J, Berry E, Young G, Rothwell P, Roditi G, Gough M, Brennan A, Bamford J, Best J. Accurate, practical and cost-effective assessment of carotid stenosis in the UK. *Health Technol Assess*. 2006;10:iii–iv, ix–x, 1–182.